

# Exploring senescent chondrocytes during aging: sleeper AGEnts of osteoarthritis

Boone, I.

#### Citation

Boone, I. (2025, October 17). Exploring senescent chondrocytes during aging: sleeper AGEnts of osteoarthritis. Retrieved from https://hdl.handle.net/1887/4273547

Version: Publisher's Version

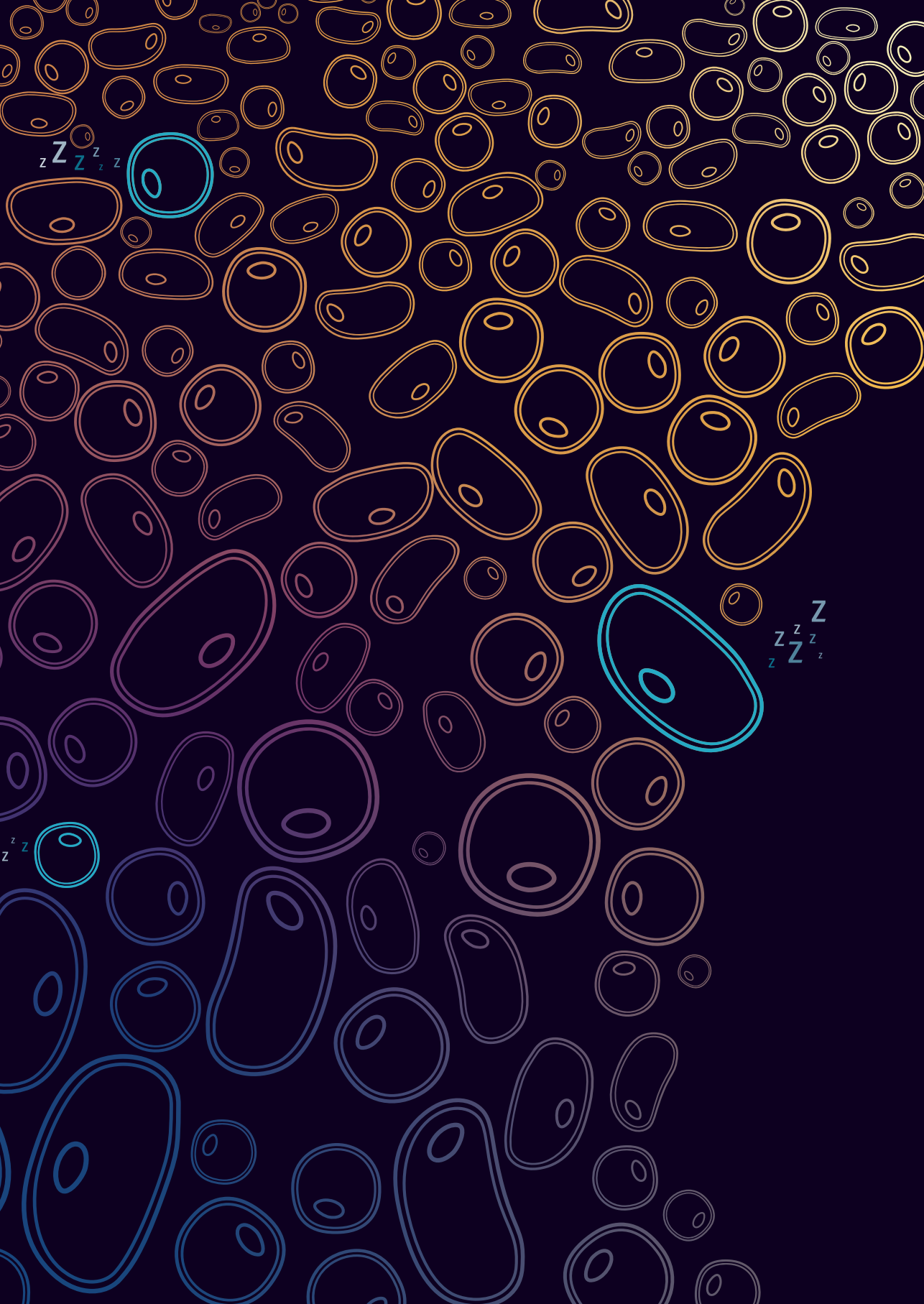
Licence agreement concerning inclusion of doctoral

License: thesis in the Institutional Repository of the University

of Leiden

Downloaded from: <a href="https://hdl.handle.net/1887/4273547">https://hdl.handle.net/1887/4273547</a>

**Note:** To cite this publication please use the final published version (if applicable).





# Development of reliable and highthroughput human biomimetic cartilage and bone models to investigate senescence and develop personalized treatments for OA

I. Boone<sup>1</sup>, E. Houtman<sup>1</sup>, M. Tuerlings<sup>1</sup>, J.J. van den Berg<sup>1</sup>, J. Lehmann<sup>2</sup>, P.L.J. de Keizer<sup>2,3</sup>, R.G.H.H. Nelissen<sup>4</sup>, I. Meulenbelt<sup>1\*</sup>

<sup>1</sup>Dept. of Biomedical Data Sciences, Section Molecular Epidemiology, Leiden University Medical Center, Leiden, The Netherlands

<sup>2</sup>Center for Molecular Medicine, Division of Laboratories, Pharmacy and Biomedical Genetics, University Medical Center Utrecht, Utrecht, The Netherlands

<sup>3</sup>Cleara Biotech B.V., Utrecht, The Netherlands

<sup>4</sup>Dept. of Orthopaedics, Leiden University Medical Center, Leiden, The Netherlands

\* Corresponding author

### **Abstract**

To facilitate effective preclinical testing of senescence treatments for osteoarthritis (OA), we have created reliable biomimetic and high-throughput models using aged human joint tissues. Moreover, concerns regarding scalability led to the concurrent development of a high-throughput human senescence neo-cartilage organoid model.

Osteochondral explants and cells for the cartilage organoid model were isolated from patients undergoing joint replacement surgery due to OA. To induce senescence, explants and pellets were subjected to radiation and/or mechanical loading. Samples were harvested, gene expression of relevant senescent and cartilage genes were measured using RT-qPCR and protein expression was evaluated using IHC.

A general senescence phenotype was induced by the perturbations, visible with the SA- $\beta$ -gal staining. In depth gene expression analysis revealed that hyper physiological mechanical loading upregulated gene expression of *IL8* and *SERPINE1*, marking a SASP model. Irradiation upregulated *CDKN1A*, encoding p21, and downregulated *LMNB1*, marking a cell cycle arrest model with absence of a SASP response. Combining the two perturbations showed upregulation of *CDKN1A*, *IL8* and *SERPINE* and downregulation of *LMNB1*, marking a complementary senescence model. The high-throughput human *in-vitro* cartilage organoid senescence model showed similar effects as the irradiation explant model.

In this study, we present a variety of senescence models of human aged chondrocytes that allows for rapid initial screening of anti-senescence compounds in high-throughput, as well as, in depth characterization of post-mitotic aged chondrocytes prone to OA pathophysiology. This research advances the development of essential personalized therapeutics for OA.

#### **Keywords**

 $Osteo arthritis \mid Cellular \ senescence \mid preclinical \ models \mid osteo chondral \ explants \mid cartilage \ organoids$ 

## Introduction

Osteoarthritis (OA) is a painful age-related degenerative joint disease that has been shown to contribute to disability and loss of quality of life. With 300 million people suffering from OA worldwide, it is the cause of the largest risk to mobility disability in patients 65 years or older <sup>4,5</sup>. Despite this burden there currently are no effective treatment options available, with pain relief and end stage joint replacement surgery as sole therapeutic option <sup>6</sup>. The backlog in effective therapy development is among others, due to a lack of insight into the diversity of the OA pathophysiology.

Cellular senescence, a hallmark of ageing is an emerging player in the OA pathophysiological process <sup>7</sup>[5]. Senescence itself is considered a heterogeneous cellular strategy to avoid cell death upon environmental stressors and is classically defined by a permanent cell cycle arrest, induced by the expression of the cell cycle inhibitors p16 and p21. Additionally, senescent cells are known for secreting a damaging and proactive inflammatory profile called the senescence associated secretory phenotype (SASP) <sup>8,9</sup>. Despite the fact that cell cycle arrest is an important marker of senescence, postmitotic cells, such as chondrocytes, also undergo cellular senescence. In postmitotic cells, however, the specific role of cell cycle arrest as induced by p16 and p21, is less well characterized nor understood <sup>8-11</sup> or even simply ignored <sup>12,13</sup>.

Notably, the field has effectively developed multiple compounds to treat cellular senescence by selectively killing senescent cells (senolytics) or modifying their SASP behavior (senomorphics) <sup>14</sup> and as such has brought new hope to treat degenerative age-related diseases <sup>9,13,15</sup> including OA <sup>16,17</sup>. Effective preclinical testing of senolytics and/or senomorphics in OA, however, requires human preclinical tissue models that faithfully accommodate the diversity in senescence in aged post-mitotic joint tissues. Notable in this respect is that we previously, set up a human aged osteochondral explant model utilizing macroscopically preserved cartilage with underlying bone isolated from joint replacement surgeries due to OA. These explants have been shown to be reliable human joint tissue model prone to OA pathophysiology upon environmental perturbations such as hyper physiological mechanical stress <sup>18,19</sup>. Importantly, hyper physiological mechanical stress in this model evoked chondrocyte senescence as marked by genes such as *GADD45A* and *SERPINE1* <sup>18</sup>. On a different note, ionizing radiation has been used previously to induce senescence in a wide range of different cell cultures <sup>20-23</sup>. Despite the fact that these human osteochondral explants reliably mimic the human OA pathophysiological process, the scalability of the model is a concern.

In the current study, we set out to exploit the aged human *ex-vivo* osteochondral explant model to characterize aspects of senescence in (post-mitotic) joint tissues. To evoke senescence, we applied hyper physiological mechanical stress and ionizing radiation to induce cellular senescence and characterized the cellular senescent phenotype of joint tissues. To address scalability, a scalable 3D human neo-cartilage organoid model was set up using ionizing radiation. This research could further advance the field of precision medicine for OA patients.

### **Methods**

### Osteochondral Explants and human in-vitro cartilage organoid model

Osteochondral explants and cells were taken from joints obtained from OA patients in the RAAK study. Explants were taken from the condyles of knee joints for the osteochondral explant culture as described previously <sup>18,19</sup>. In short, biopsies were taken from the macroscopically normal cartilage from OA patients and washed in PBS. Next, the explants were cultured in serum-free chondrogenic differentiation medium

The human primary articular chondrocytes (hPACs) were collected and cultured as described previously <sup>24</sup>. In short, macroscopically normal cartilage was treated overnight in medium with collagenase type 1 (Worthington) and cultured in serum-free chondrogenic differentiation medium. Subsequently, the human *in-vitro* cartilage organoids were formed using 500 g centrifugal forces on a 96 wells plate and cultured in serum-free chondrogenic differentiation medium. In this experiment a total of 142 explants from 29 donors were included and cells from 3 additional donors were used for the human *in-vitro* cartilage organoids. Donor characteristics are described in Supplementary Table S1. Additional details are available in the Supplementary methods.

### Irradiation and loading regime

As seen in Figure 1, three days after extraction, explants were placed in sterile PBS and irradiated with 20 Gy (Yxlon, Germany). Subsequently, after 5 days, 65% dynamic unconfined compression was applied using the MACH-1 (Biomomentum Inc., Laval, QC, Canada) apparatus for 4 days. At day 12, the explants were harvested for IHC and RNA analysis. As seen in Figure 1, the human in-vitro cartilage organoids were exposed to 10 or 20 Gy ionizing radiation on day 7 of the culture and on day 10 the cartilage organoids were harvested for RNA analysis. In total 143 osteochondral explants were used from 29 donors, divided in control (n=31 osteochondral explants, N=29 donors), irradiation (n = 16 osteochondral explants and N = 12 donors), hyper physiological mechanical loading (n = 20 osteochondral explants and N = 18 donors) and combination group(n = 42 osteochondral explants and N = 29 donors). Additional details are available in the Supplementary methods.

### Gene expression

Osteochondral explants and human *in-vitro* cartilage organoids were processed and RNA was extracted as described previously <sup>18,19</sup>. In summary, the cartilage and bone of the osteochondral explants were separated and pulverized using a Mixer mill 200 (Retch, Germany) in TRIzol reagent. RNA was extracted using the RNeasy Mini Kit (Qiagen, GmbH, Hilden, Germany). The quantity of RNA was assessed and cDNA synthesis was performed. Gene expression was measured using RT-qPCR, with the Biomark™ 96.96 Dynamic Arrays (Fluidigm) according to the manufacturer's protocol and with the QuantStudio 6 Real-Time PCR system (Applied Biosystems). *POU6F1* and *HECTD3* were used as housekeeping genes. All genes measured using RT-qPCR and their primer sequence are listed in Supplementary Table S2.

### Statistical analysis

Statistical tests were performed using SPSS (v.29). Significance was determined using unpaired Generalized Estimating equations (GEE) with multivariate analysis. Genes were taken as dependent

variable, models were taken as independent variable and there was corrected for RT-qPCR analysis type and donor. Controls were taken as baseline.

### Histology

For the senescence associated beta galactosidase (SA- $\beta$ -gal) staining, a slice of the explants was washed with PBS and fixed for 15 minutes at 4 dC using 4% formaldehyde with 0.5% glutaraldehyde. The explants were washed and incubated for 24 hours at 37dC with the staining solution at pH 6 as described previously  $^{25}$ . Samples were decalcified, embedded and sectioned. Slides were washed and counterstained with nuclear fast red (Sigma) for 5 minutes. Slides were imaged with the Zeiss Axioscan Z1 slide scanner, using a 10x magnification. Images were processed and quantified using ImageJ (v.1.53c). When chondrocytes were blue they were considered SA- $\beta$ -gal positive. The total number of SA- $\beta$ -gal positive cells were counted and averaged. Additional details are available in the Supplementary methods.

For the cartilage quality score (Mankin score), explants were fixed for 24 hours at 4°C, subsequently decalcified and sectioned. Tissue sections were stained with Haematoxylin & Eosin Y (H&E) or Toluidine Blue (Sigma-Aldrich), as described previously <sup>18</sup> and scored for cartilage integrity by using the Mankin score and two independent reviewers <sup>26</sup>.

To indicate apoptotic cells in the tissue, explants were decalcified, sectioned and the Click-iT<sup>™</sup> Plus TUNEL assay kit was used (Invitrogen). In short, first a TdT reaction was performed, followed by the Click-iT<sup>™</sup> plus reaction and DAPI was used as counter stain. Slides were imaged with the Zeiss Axioscan Z1 slide scanner, using a 10x magnification. Images were processed using ImageJ (v.1.53c). Per tissue, 4 random areas were selected and averaged per condition (N= 2 donors). The

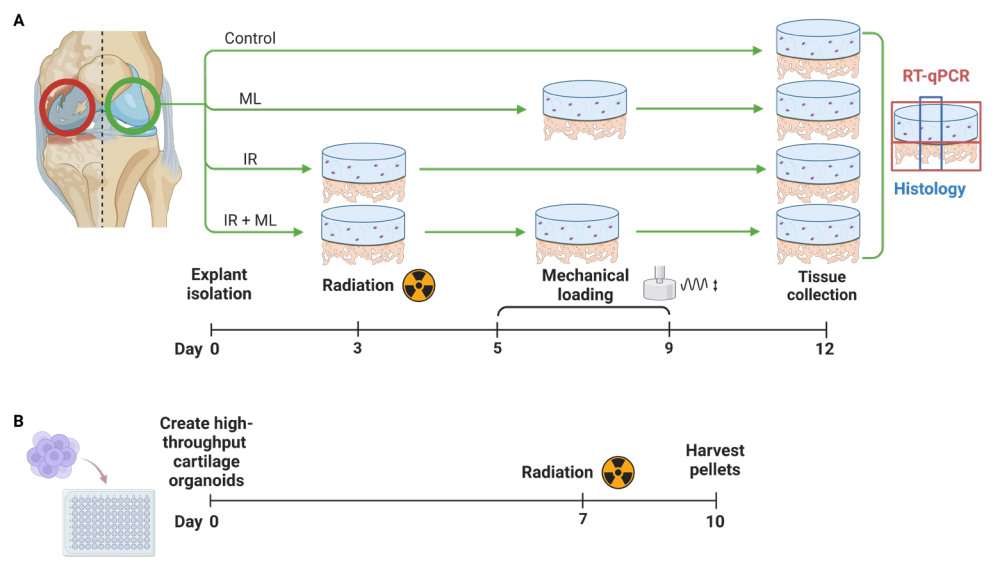


**Figure 1** - Experiment timeline of **A**, the osteochondral explants; timeline of the irradiation (IR), hyper physiological mechanical loading (ML) and combination (IR + ML) models. Bone and cartilage were separated for gene expression analysis. Before separation, cross-sections were taken for histology. **B**, The high-throughput human neo-cartilage mini pellets; timeline of the irradiation and harvest of the human in-vitro cartilage organoid model. Complete pellets were taken for gene expression analysis and histology. Created with BioRender.com

TUNEL-positive cells were counted as apoptotic cells and the DAPI- positive cells were used as the total number of cells. Additional details are available in the Supplementary methods.

### **Results**

### Study characteristics of the aged human OA osteochondral explants

We here characterized 3 different senescence-associated perturbing regimes in the aged human osteochondral explants harvested from preserved OA knee tissues. Using ionizing radiation and hyper physiological mechanical loading, we created a hyper physiological mechanical loading model, a irradiation model and a combination model where irradiation and the hyper physiological mechanical loading are combined. To assure robust comparisons between the models, multiple osteochondral explants were harvested from preserved areas of the N=29 donor knee joints as outlined previously <sup>18</sup>, and evenly distributed across the experimental groups. As such and as shown in Supplementary Table S1 and Supplementary Figure S1, age, sex, OA severity (KL score, pre-operative) and histological quality of articular cartilage (Mankin scores) were similar across the models.

### Characterization of general senescence in the models

To assess the level of senescence in the different models created with hyper physiological mechanical loading and ionizing radiation, we applied the commonly used SA- $\beta$ -gal staining, indicating senescent cells (Figure 2). Although the irradiation model (Mean = 69%, SD = 6%, Figure 2) showed similar levels of senescence as the untreated explants (Mean = 75%, SD = 7%), we confirmed increasing levels of senescence in hyper physiological loading model (Mean = 85%, SD = 9%) and the combination model (Mean = 95%, SD = 3%). Together SA- $\beta$ -gal staining confirmed induction of general senescence in the osteochondral explant model by irradiation and/ or mechanical loading.

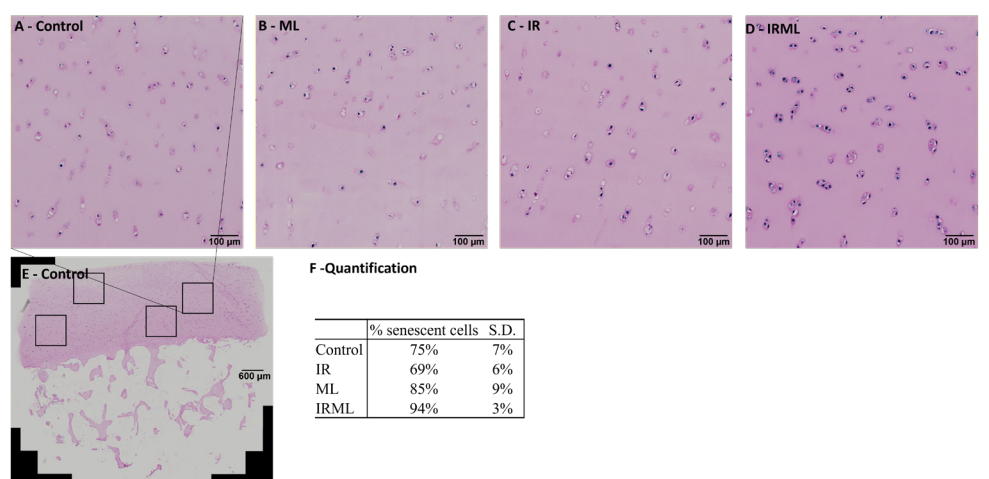


**Figure 2** - Representative images and quantification of SA-B-gal staining in **A**, Control explant. **B**, Hyper physiological mechanical loading model. **C**, Irradiation model. **D**, Combination model. **E**, overview image of entire control explant, scale bar is 600 µm. Scale bar is 100 µm in A-D. For the quantification, average of 8 squares from two histological sections of one donor were used. N=1 donor and n= 2 histological sections. S.D, standard deviation. IR = irradiation model, ML = hyper physiological mechanical loading model, Combi = Combination model

# In depth characterization of senescence in the hyper physiological mechanical stress model

To study specific aspects of the senescence phenotypes i.e. markers of the classical irreversible cell cycle arrest and/or SASP <sup>27</sup>, we next characterized downstream effects on the cellular phenotype of chondrocytes in response to the senescence inducing perturbations irradiation and/or hyper physiological mechanical stress by RT-qPCR. Hereto, we assessed gene expression changes of specific genes that mark these different aspects of the senescence phenotype in control and perturbed osteochondral explants. To indicate tissue state, we used *COL2A1* and *ACAN* for cartilage anabolism, *COL1A1* for bone anabolism, *DMP1* and *MEPE* as osteocyte markers, *CTSK* as osteoclast marker and *RUNX2* and *ALPL* as osteoblast markers. We explored the classical cell cycle arrest profile using *CDKN1A*, *LMNB1*, and the SASP profile using *IL6*, *IL8* and *SERPINE1*.

Hyper physiological mechanical loading was used as a perturbation to induce senescence in the osteochondral explants. As shown in Table 1 and 2 and in Supplementary Figure S2 and S3, this model resulted in a particular and significant response of the SASP profile in both cartilage and bone. In cartilage, mainly *IL8* (beta=1.6, P=2.2x10<sup>-02</sup>) and *SERPINE1* (beta=0.5, P=7.8x10<sup>-03</sup>) responded with an upregulation after mechanical loading. In bone, we observed a stronger upregulation than in cartilage, with mainly *IL6* (beta=0.9, P=4.7x10<sup>-02</sup>) and *MMP13* (beta=2.8, P=5.4x10<sup>-14</sup>) as potent markers. As seen in Figure 3A/B, there was no effect in the classical cell cycle arrest profile (e.g. *CDKN1A* and *LMNB1*) or tissue state genes of both cartilage (e.g. *COL2A1*, Table 2) and bone (e.g. *COL1A1*, Table 3), supporting the cartilage quality scoring. Together, these data indicated that the hyper physiological mechanical loading model resulted mainly in the upregulation of a SASP profile with the absence of a classical cell cycle arrest profile.

### In depth characterization of senescence in the irradiation model

Ionizing radiation was used as perturbation to induce senescence in the osteochondral explants. This model resulted in a particular and significant response of the classical cell cycle arrest profile in both cartilage and bone. In cartilage, mainly CDKN1A (beta=1.3, P=3.7x10<sup>-09</sup>, Figure 3A) showed a significant upregulation after irradiation of the osteochondral explants. In bone, all classical cell cycle arrest markers, e.g. CDKN1A, CDKN2A (beta=1.8, P=1.1x10<sup>-26</sup> and beta=1.4, P=9.0x10<sup>-07</sup> respectively, Table 2 and Figure 3B) showed a strong significant upregulation of the classical cell cycle arrest profile. There was no effect on tissue state genes of cartilage (e.g. COL2A1, beta=0.2, P=7.4x10<sup>-01</sup>, Table 1). As seen in Table 2 and Supplementary Figure S3, in bone, we observed a decrease in osteocyte osteoclast specific markers (DMP1, beta=-1.2, P=4.1x10<sup>-03</sup>), osteoblast markers (CTSK, beta=-1.5, P=7.1x10<sup>-08</sup>) and osteoblast markers (ALPL, beta=-2.3, P=4.1x10<sup>-10</sup>), as well as bone anabolism marker (COL1A1, beta=-2.4, P=4.0X10<sup>-15</sup>). While we observed no increase in apoptotic bone cells (Supplementary Table S3). These findings indicated that the irradiation model resulted mainly in the upregulation of the classical cell cycle arrest profile with the absence of a SASP response.

### In depth characterization of senescence in the combination model

Both hyper physiological mechanical loading and irradiation were combined to induce senescence in the combination model. This model resulted in the upregulation of a SASP profile and classical cell cycle arrest profile. As shown in Table 1 and Figure 3A, in cartilage, the upregulated classical cell cycle arrest profile, showing modest effect sizes, mainly included *CDKN1A* and *LMNB1* (beta=1.5,

 $P=7.8\times10^{-70}$  and beta=-0.7,  $P=4.4\times10^{-02}$ , respectively). While the upregulated SASP profile consisted of IL6, IL8 and SERPINE1 (beta=2.8,  $P=1.3\times10^{-02}$ , beta=1.3,  $P=6.6\times10^{-03}$  and beta=0.7,  $P=5.7\times10^{-04}$ , respectively), similar as in the separate models. There was no effect in tissue state genes of cartilage (e.g. COL2A1, beta=-0.3,  $P=2.4\times10^{-01}$ , Table 1). As seen in Table 2 and Supplementary Figure S3, in bone, we observed a complete response of the classical cell cycle arrest profile, resulting in a more robust upregulation of CDKN1A, CDKN2A and LMNB1 (beta=1.9,  $P=2.0\times10^{-66}$ , beta=1.2,  $P=8.3\times10^{-10}$  and beta=-2.3,  $P=4.9\times10^{-45}$ , respectively Supplementary Figure S2), compared to cartilage. As seen in Figure 3B, the significant upregulation of the SASP profile in bone consisted mainly of SERPINE1 (beta=0.5,  $P=5.1\times10^{-04}$ ) and MMP13 (beta=1.4,  $P=2.7\times10^{-05}$ ).

Similar to the irradiation model, we observed a decrease in bone type specific and anabolism genes (Table 2), while no difference in the apoptosis level of these cells was measured (Supplementary Table S3). These results demonstrate that hyper physiological mechanical loading and irradiation resulted in a robust upregulation of a complementary senescence profile rather than enhancing specific senescence aspects.

# Cell cycle arrest profile in the high-throughput neo-cartilage mini pellet model

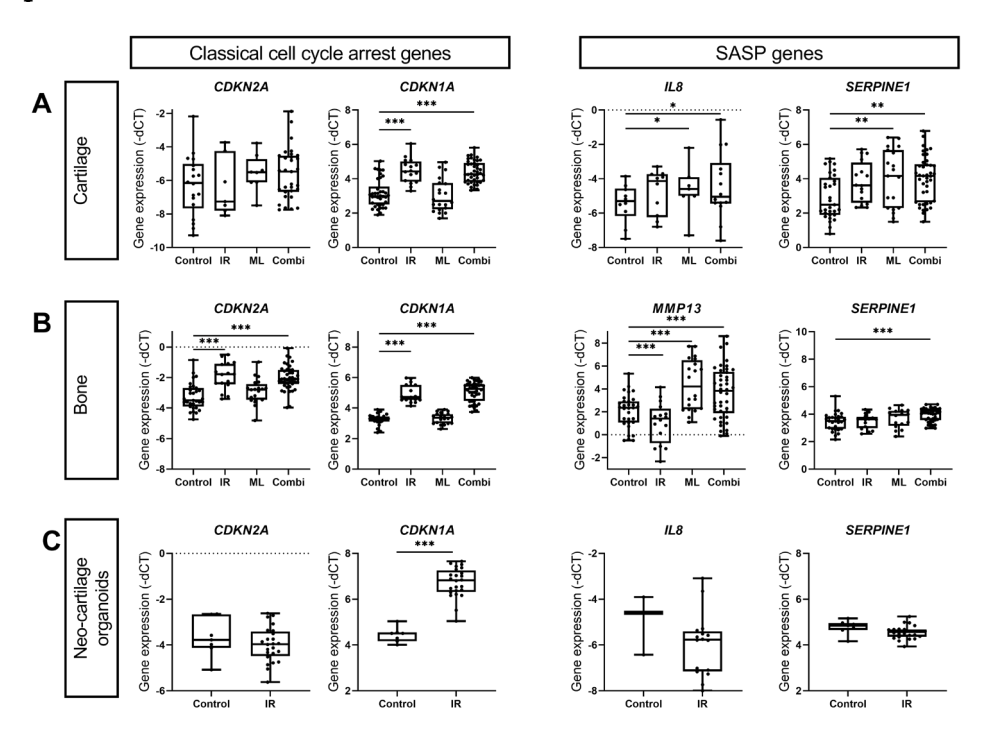


**Figure 3** - Gene expression of the cell cycle arrest profile and SASP genes **A**, in the cartilage of the hyper physiological mechanical loading (n=17-51 osteochondral explants and N=12-29 donors) and in the irradiation groups (n=16-47 osteochondral explants and N=11-29 donors). **B**, in the bone cartilage of the hyper physiological mechanical loading (n=45-51 osteochondral explants and N=27-29 donors) and in the irradiation groups (n=45-47 osteochondral explants and N=28-29 donors). **C**, in the high-throughput human neo-cartilage mini pellet model (n=19-31 mini pellets and N=3 donors). ML=hyper physiological mechanical loading model, IR=irradiation model, \*P<0.05, \*\*P<0.01, \*\*\*P<0.001.

The development of disease modifying OA drugs requires not only a high quality biomimetic senescence model, but also a scalable model that accommodates high-throughput screening of compounds. We here developed a high-throughput human senescence *in-vitro* organoid model of cartilage senescence using ionizing radiation in 96 well format. Age, sex and OA severity were similar between controls and the senescence model (Supplementary table S1). The high-throughput mini neo-cartilage senescence model showed highly similar results as compared to the cell cycle arrest model. As seen in Figure 3C and Supplementary Table S4, we observed a significant upregulation of the classical cell cycle arrest profile, characterized by *CDKN1A*, *GADD45A* and *LMNB1* (beta 2.3, P=1.6 x10<sup>-33</sup>, beta 1.2, P=4,6 x10<sup>-18</sup> beta -2.9, P=3.7x10<sup>-11</sup>, respectively) and no significant response of the SASP profile. In addition, we observed significant downregulation of cartilage quality markers *COL2A1* and *ACAN* (beta -0.5 , P=2.5x10<sup>-02</sup> and beta -1.0, P=1.6x10<sup>-05</sup>, respectively, Supplementary Table S4). Indicating that the high-throughput mini neo-cartilage senescence model is highly similar to cell cycle arrest model.

# Distinguishing between gene expression profiles of senescence and OA pathophysiology

Since there is overlap in gene expression such as *IL6*, *IL8*, *MKI67*, and *SERPINE1* that mark senescent and OA joint tissue cells <sup>27</sup>, we compared the expression pattern of the here studied genes to the applied senescence inducing perturbations in preserved cartilage and bone (Table 1 and 2) with those previously reported in OA lesioned relative to preserved cartilage and bone. As shown in Supplementary table S5, the SASP factors *IL6* and *IL8* that were highly responsive to the senescence inducing factors, appeared not to be upregulated in lesioned OA affected bone and cartilage. Vice versa, *MKI67* appeared not responsive to the senescence inducing mechanical loading, yet was significantly upregulated in OA chondrocytes. *SERPINE1* was highly responsive to senescence inducing as well as highly significantly upregulated in lesioned compared to preserved OA affected bone and cartilage <sup>1-3</sup>. As such we conclude that senescence and OA joint tissue cells have distinct gene expression patterns.

Table 1 - Effect of the hyper physiological mechanical loading and irradiation perturbation on cartilage of the osteochondral explant.

	Hyper physiological mechanical loading model		Irradiatio	Irradiation model		Combination model			
	FC (SD)	Beta	P-value	FC (SD)	Beta	P-value	FC (SD)	Beta	P-value
Cartilage anabolism	1								
COL2A1	0.6 (1.5)	0.3	5.2x10 <sup>-01</sup>	0.8 (0.6)	0.2	7.4x10 <sup>-01</sup>	0.6 (0.6)	-0.3	2.4x10 <sup>-01</sup>
ACAN	1.0 (0.4)	-0.2	4.2x10 <sup>-01</sup>	0.9 (0.5)	-0.1	5.5x10 <sup>-01</sup>	0.8 (0.5)	-0.1	5.6x10 <sup>-01</sup>
Positive senescence	markers								
CDKN1A	1.3 (0.6)	0.1	3.6x10 <sup>-01</sup>	2.7 (1.4)	1.3	3.7x10 <sup>-09</sup>	2.7 (1.0)	1.5	7.8x10 <sup>-70</sup>
CDKN2A	0.8 (1.7)	1.0	9.1x10 <sup>-02</sup>	0.8 (0.8)	-0.6	5.5x10 <sup>-01</sup>	1.8 (4.4)	0.9	7.5x10 <sup>-02</sup>
GADD45A	0.9 (0.4)	-0.1	5.6x10 <sup>-01</sup>	2.0 (1.3)	0.7	1.3 x10 <sup>-02</sup>	1.4 (1.2)	0.4	6.1 x10 <sup>-02</sup>
Negative senescence	e markers								
MKI67	0.8 (1.8)	0.1	9.3x10 <sup>-01</sup>	0.1 (1.0)	-2,7	2.2 x10 <sup>-02</sup>	0.1 (1.2)	-3.6	3.4 x10 <sup>-04</sup>
LMNB1	1.0 (1.0)	0.1	8.8x10 <sup>-01</sup>	0.5 (0.6)	-0.9	1.9x10 <sup>-01</sup>	0.7 (1.2)	-0.7	4.4x10 <sup>-02</sup>
HMGB1	1.1 (0.5)	0.2	4.3x10 <sup>-01</sup>	1.3 (0.2)	0.5	1.1x10 <sup>-01</sup>	1.4 (3.8)	0.4	1.5x10 <sup>-01</sup>
SASP markers									
IL6	3.6 (11.8)	3.9	5.8x10 <sup>-02</sup>	4.7 (6.2)	1.0	4.6x10 <sup>-01</sup>	3.8 (18.5)	2.8	1.3x10 <sup>-02</sup>
IL8	2.0 (4.5)	1.6	2.2x10 <sup>-02</sup>	1.1 (0.9)	0.1	8.5x10 <sup>-01</sup>	1.8 (1.6)	1.3	6.6x10 <sup>-03</sup>
SERPINE1	1,.9 (1.6)	0.5	7.8x10 <sup>-03</sup>	1.4 (1.0)	0.6	1.1x10 <sup>-01</sup>	1.8 (1.3)	0.7	5.7x10 <sup>-04</sup>
IGFBP3	0.3 (1.5)	-2.2	1.5x10 <sup>-03</sup>	0.4 (1.1)	-0.6	6.1x10 <sup>-01</sup>	0.2 (1.6)	-2.2	5.7x10 <sup>-04</sup>
IGFBP6	0.4 (0.2)	-1.1	3.9x10 <sup>-05</sup>	1.3 (1.0)	-0.1	6.0x10 <sup>-01</sup>	0.4 (0.4)	-1.4	1.9x10 <sup>-10</sup>
MMP3	0.8 (0.3)	-0.4	1.0x10 <sup>-01</sup>	1.0 (0.4)	0.4	4.3x10 <sup>-01</sup>	0.6 (0.3)	-0.6	3.3x10 <sup>-02</sup>
MMP13	1.5 (4.8)	-0.1	8.9x10 <sup>-01</sup>	0.7 (1.4)	-0.9	5.8x10 <sup>-01</sup>	0.7 (2.8)	-0.7	3.0x10 <sup>-01</sup>

Notes: GEE test,  $FC=2^{-diCT}$ , SD= standard deviation, Beta= estimate of the GEE test and baseline are controls. P-value<0.05 is considered significant, n= 16-51 osteochondral explants, N= 12-29 donors.

Table 2 - Effect of the hyper physiological mechanical loading and irradiation perturbation on bone of the osteochondral explant.

	Hyper physiological mechanical		1	rradiati	on model	Combination model			
	loading model					DC (OD) D .			
	FC (SD)	Beta	P-value	FC (SD)	Beta	P-value	FC (SD)	Beta	P-value
Bone anabolism									
COL1A1	1.0 (0.8)	0.2	3.5x10 <sup>-01</sup>	0.3 (0.2)	-2.4	4.0x10 <sup>-15</sup>	0.4 (0.6)	-1.3	1.2x10 <sup>-08</sup>
Osteocyte markers									
DMP1	1.0 (0.7)	-0.6	2.1x10 <sup>-02</sup>	0.7 (0.3)	-1.2	4.1x10 <sup>-03</sup>	0.7 (0.5)	-0.6	4.9x10 <sup>-02</sup>
MEPE	1.5 (1.9)	0.4	8.5x10 <sup>-02</sup>	1.9 (1.0)	0.3	3.2x10 <sup>-01</sup>	2.1 (1.4)	1.1	6.5x10 <sup>-06</sup>
Osteoclast markers									
CTSK	1.2 (1.4)	0.1	7.5x10 <sup>-01</sup>	0.5 (0.3)	-1.5	7.1x10 <sup>-08</sup>	0.6 (0.5)	-0.8	1.7x10 <sup>-04</sup>
Osteoblast markers									
RUNX2	1.2 (0.4)	0.2	8.1x10 <sup>-02</sup>	0.7 (0.2)	-0.8	4.3x10 <sup>-06</sup>	0.8 (0.3)	-0.3	1.1x10 <sup>-02</sup>
ALPL	1.0 (0.8)	0.1	5.8x10 <sup>-01</sup>	0.3 (0.3)	-2.3	4.1x10 <sup>-10</sup>	0.3 (0.3)	-1.7	8.5x10 <sup>-13</sup>
Positive senescence	markers								
CDKN1A	1.1 (0.3)	0.0	5.9x10 <sup>-01</sup>	3.6 (1.5)	1.8	1.1x10 <sup>-26</sup>	3.6 (1.9)	1.9	2.0x10 <sup>-66</sup>
CDKN2A	1.2 (0.6)	0.3	1.6x10 <sup>-01</sup>	2.6 (1.8)	1.4	9.0x10 <sup>-07</sup>	2.4 (1.7)	1.2	8.3x10 <sup>-10</sup>
GADD45A	0.9 (0.2)	-0.6	2.2x10 <sup>-04</sup>	1.9 (0.3)	0.9	6.3 x10 <sup>-11</sup>	1.8 (0.4)	0.9	2.0 x10 <sup>-0</sup>
Negative senescence	markers								
MKI67	0.8 (0.5)	-0.4	2.3 x10 <sup>-01</sup>	0.1 (0.1)	-4.0	1.5 x10 <sup>-20</sup>	0.1 (0.2)	-3.4	1.4 x10 <sup>-4</sup>
LMNB1	1.1 (0.4)	-0.2	2.5x10 <sup>-01</sup>	0.2 (0.1)	-2.8	4.5x10 <sup>-35</sup>	0.2 (0.2)	-2.3	4.9x10 <sup>-45</sup>
HMGB1	1.1 (0.4)	-0.1	7.0x10 <sup>-01</sup>	0.8 (0.2)	-0.4	2.5x10 <sup>-02</sup>	0.8 (0.3)	-0.3	1.5x10 <sup>-02</sup>
SASP markers									
IL6	1.2 (1.3)	0.9	4.7x10 <sup>-02</sup>	1.8 (2.3)	0.4	2.0x10 <sup>-01</sup>	2.6 (6.2)	1.3	1.6x10 <sup>-04</sup>
IL8	1.3 (4.4)	0.4	1.9x10 <sup>-01</sup>	1.0 (0.4)	0.3	3.6x10 <sup>-01</sup>	1.4 (3.6)	0.3	1.8x10 <sup>-01</sup>
SERPINE1	1.4 (0.7)	0.2	2.8x10 <sup>-01</sup>	1.1 (0.3)	0.1	5.5x10 <sup>-01</sup>	15 (0.9)	0.5	5.1x10 <sup>-04</sup>
IGFBP3	0.8 (0.5)	-0.7	1.3x10 <sup>-04</sup>	1.0 (0.3)	0.1	6.9x10 <sup>-01</sup>	0.7 (0.4)	-0.6	6.4x10 <sup>-04</sup>
IGFBP6	0.8 (0.5)	-0.5	3.8x10 <sup>-03</sup>	1.5 (1.0)	0.5	1.3x10 <sup>-01</sup>	1.4 (0.7)	0.3	6.5x10 <sup>-02</sup>
MMP3	1.5 (14.5)	0.2	7.4x10 <sup>-01</sup>	3.2 (3.7)	0.6	5.1x10 <sup>-01</sup>	2.5 (24.1)	1.5	1.1x10 <sup>-02</sup>

**Notes:** GEE test, FC=2-ddCT, SD= standard deviation, Beta= estimate of the GEE test and baseline are controls, P-value<0.05 is considered significant, n = 16-51 osteochondral explants, N = 12-29 donors.

### **Discussion**

To allow in-depth preclinical studies targeting OA-associated senescence, we set up and characterized diverse aspects of cellular senescence in joint tissues. Hereto we exploited our human aged macroscopically normal osteochondral explants model 19, while applying the senescent relevant perturbations hyper-physiological mechanical stress 18 and irradiation 21,23,28. Irradiation evoked in both the cartilage and bone compartment a cell cycle arrest profile, marked particularly by the upregulation of CDKN1A, encoding p21. On the other hand, hyper physiological mechanical loading evoked in the cartilage compartment a SASP profile, marked particularly by the upregulation of IL8 and SERPINE1. Combining these two perturbations evoked a complementary senescence profile, marked by the upregulation of both CDKN1A, representing a cell cycle arrest profile, and IL6, IL8 and SERPINE1, representing a SASP phenotype. The introduction of these models allows for further exploration of the specific downstream aspects of senescence in the onset of the OA pathophysiology and facilitates both general and selective testing of senolytics and/ or senomorphics 14. To accommodate high-throughput we, in parallel, miniaturized our previously set up 3D in-vitro cartilage organoid model. Importantly, these human biomimetic senescence models contribute to the guiding principles of reduction, refinement, and replacement of animal models.

In these models, a stronger induction of cell cycle arrest profile was measured in bone when compared to cartilage, this can be explained by the post-mitotic nature of chondrocytes and the active proliferative nature of bone cells hence prone to go into cell cycle arrest <sup>29</sup>. In our results, this is confirmed mainly by the strong response of the classical cell cycle arrest profile in bone tissue e.g., *CDKN2A* upregulation and *LMNB1* downregulation. In addition, we observed different SASP profiles responding to the senescent triggers in bone and cartilage. *IL6* and *SERPINE1* were recognized as consistent SASP markers across models, *IL8* and *MMP13* were specific SASP markers for cartilage and bone respectively. This supports the notion that SASP profile is heterogeneous across tissue types and should be targeted differently <sup>30</sup>.

In the complementary senescence model, we observed a response of complete senescence profile, consisting of both the cell cycle arrest and the SASP profile. In cartilage and bone, these senescent profiles both respond to the same extend in the complimentary senescence model. This indicates that the two senescence perturbations of the complementary senescence model act separately rather than combine and enhance their respective senescence effects. Henceforth, the complementary senescence model is suitable to study the role of broad senescence phenotype in the onset of OA pathophysiology as well as for the testing of both senolitics and or senomorphic compounds.

In this study we used the commonly used SA- $\beta$ -gal at a pH of 6  $^{25}$ , to indicate overall levels of senescence. An unexpected high amount (75%) of intrinsic senescent cells in articular cartilage of these control human explants was observed, that are per definition aged but structurally unaffected by the OA pathophysiology process  $^2$ . The high amount of senescence cells in control samples could highlight a profound accumulation of cellular senescence with age in articular cartilage, or that SA- $\beta$ -gal perse is less suitable to sensitively mark classical cell cycle arrest senescence in postmitotic tissues such as articular cartilage. Since we showed that the different senescence inducing perturbations applied to our model evoked consistent and specific aspects of cellular

senescence by gene expression patterns, we advocate that SA- $\beta$ -gal indeed is less suitable to mark senescence in postmitotic tissues such as articular cartilage. Having said this, the fact that SA- $\beta$ -gal predominantly marked chondrocytes in the combination model (with up to 95% of cells showing SA- $\beta$ -gal positivity) suggests that irradiation induces dysfunctional chondrocytes, when these cells are subsequently subjected to hyper-physiological stress, they may lose their ability to effectively respond to additional damage. In any case these results need to be verified in larger sample sizes and possibly in healthy articular chondrocytes.

Given the overlap between in genes that appear responsive to OA pathophysiology in cartilage <sup>1</sup>, bone <sup>3</sup> and the SASP <sup>27</sup>, we also would like to stress that the models presented here are specific and consistent to the senescence inducing perturbations applied. This is illustrated by the defined yet different expression patterns of genes such as *IL6*, *IL8*, *MKI67*, and *SERPINE1* in senescent and OA affected cartilage and bone. As such we are confident that the result of our study and senescence associated claims are robust.

Despite the fact that the classically irreversible cell cycle arrest senescent profile is marked by both p21/p53 and p16 pathways, in the cartilage compartment, irradiation evoked a strong response of particularly *CDKN1A* (p21) and a lack of response in *CDKN2A* (p16). Since this predominance of p21 associated senescence in postmitotic chondrocytes was in line with previous studies <sup>31-33</sup>, our results confirm that cell cycle arrest aspects of chondrocyte senescence particularly act via the p21/p53 pathway. Important to note in this respect is also that it was previously shown that accumulation of senescence cells in post mitotic tissues such as articular cartilage affected the capacity to respond to environmental stressors <sup>11</sup>. Together it is tempting to suggest that the accumulation of p21/p53 associated cellular senescence affects chondrocyte plasticity to respond to environmental stressors throughout life hence the propensity to enter an OA disease state.

To facilitate scalability, a high-throughput cartilage organoid model was set up, although only for cartilage, that showed similar levels of cell cycle arrest profile as the cell cycle arrest explant model; a response in *CDKN1A*. Notable was that we also observed a reduction of *COL2A1* and *ACAN* gene expression, which was absent in the explant model. This could be due to the high baseline *COL2A1* and *ACAN* expression and the absence of the native architecture in the neocartilage causing these chondrocytes to respond differently to the irradiation. Another possibility is that these chondrocytes are actively producing matrix and are more susceptible to senescence triggers and the matrix production is hampered. These results indicate that this high-throughput neo-cartilage model could be used for fast initial screening of anti-senescence compounds against the cell cycle arrest profile while the explant model could be used as a validation model for these compounds. This scalable model for therapeutics could be further explored to include humaninduced pluripotent stem cells (hiPSCs) as a stable cell source, instead of the hPACs used in this research <sup>34</sup>. Future focus will be on adding mechanical loading to this high-throughput model system to facilitate drug screenings for a broad senescence range.

A limitation of our study was that the SA- $\beta$ -gal staining could not be used to quantitatively assess the number of senescent cells in subchondral bone, due to the complex matrix of bone, and handling of the samples during sectioning. Additionally, the sample size of the SA- $\beta$ -gal staining should be increased. Moreover, since chondrocytes are embedded in a stringent extra cellular matrix, simple effective antigen retrieval methods are not possible and complex antigen retrieval methods are

required. As a result, protein staining of other senescence proteins, like p21, to complement  $SA-\beta$ -gal staining could not be performed

Finally, the TUNEL assay appeared to indicated >100% of apoptotic bone cells. We anticipate that this is caused by the fact that the TUNEL staining is known to stain fragmented nuclear DNA but also extra-nuclear fragmented DNA. When the cell is no longer intact due to apoptosis following external stimuli like hyper physiological mechanical loading, there is a possibility that the TUNEL assay has detected it as a cell, hence creating a scoring of >100%.

Taken together, we present a reliable biomimetic human joint tissue model that allows for in-depth preclinical studies targeting OA-associated senescence. Moreover, to address scalability, a high-throughput human neo-cartilage mini senescence pellet model was introduced. Together, these models facilitate effective preclinical testing strategies of senolytics and/or senomorphics in OA, while faithfully accommodating diversity in senescence in aged post-mitotic joint tissues.

# Acknowledgements

We thank all the participants of the RAAK study. The LUMC has and is supporting the RAAK study. We thank all the members of our group. We also thank Demiën Broekhuis, Enrike van der Linden, Robert van der Wal, Anika Rabelink-Hoogenstraaten, Peter van Schie, Shaho Hasan, Maartje Meijer, Daisy Latijnhouwers and Geert Spierenburg for collecting the RAAK material. We thank all participating patients and doctors at Alrijne Leiderdorp. We thank Rachid Mahdad for his contribution to the collection of joint tissue.

### **Funding**

The study was funded by VOILA – SMARTage (nr LSHM18093), the Dutch Arthritis Society (DAA\_10\_1-402) and the Dutch Scientific Research council NWO /ZonMW VICI scheme (nr. 91816631/528). Data is generated within the scope of the Medical Delta programs Regenerative Medicine 4D: Generating complex tissues with stem cells and printing technology and Improving Mobility with Technology.

#### Conflict of interest

PDK is founder, managing director and shareholder of Cleara Biotech B.V., a company developing compounds against cellular senescence.

#### **Author Contributions**

Conceptualization: IB, IM, Funding acquisition: IM, PDK, Methodology: IB, EH, MT, JVDB, JL, Resources: IM, RN, Supervision: IM, Validation: JVDB, Visualization: IB, IM, Writing—original draft: IB, IM, Writing—reviewing & editing: IB, IM, EH, MT, JVDB, JL, PDK, RN.

## References

- Hunter, D.J., D. Schofield, and E. Callander, The individual and socioeconomic impact of osteoarthritis. Nat Rev Rheumatol, 2014. 10(7): p. 437-41.
- Abramoff, B. and F.E. Caldera, Osteoarthritis: Pathology, Diagnosis, and Treatment Options. Med Clin North Am, 2020. 104(2): p. 293-311.
- 3. Kan, H.S., et al., Non-surgical treatment of knee osteoarthritis. Hong Kong Med J, 2019. 25(2): p. 127-133.
- Xie, J., et al., Cellular senescence in knee osteoarthritis: molecular mechanisms and therapeutic implications. Ageing Res Rev, 2021. 70: p. 101413.
- Jeon, O.H., et al., Senescent cells and osteoarthritis: A painful connection, in Journal of Clinical Investigation.
   2018, American Society for Clinical Investigation. p. 1229-1237.
- Coryell, P.R., B.O. Diekman, and R.F. Loeser, Mechanisms and therapeutic implications of cellular senescence in osteoarthritis. Nature Reviews Rheumatology, 2021. 17(1): p. 47-57.
- Jeon, O.H., et al., Local clearance of senescent cells attenuates the development of post-traumatic osteoarthritis and creates a pro-regenerative environment. Nat Med, 2017. 23(6): p. 775-781.
- Sapieha, P. and F.A. Mallette, Cellular Senescence in Postmitotic Cells: Beyond Growth Arrest. Trends Cell Biol, 2018. 28(8): p. 595-607.
- 9. Kirsch, V., et al., In Vitro Characterization of Doxorubicin-Mediated Stress-Induced Premature Senescence in Human Chondrocytes. Cells, 2022. 11(7): p. 1106.
- Huang, Y., et al., Senolytic Peptide FOXO4-DRI Selectively Removes Senescent Cells From in vitro Expanded Human Chondrocytes. Front Bioeng Biotechnol, 2021. 9: p. 677576.
- 11. Gasek, N.S., et al., Strategies for targeting senescent cells in human disease. Nature Aging, 2021. 1(10): p. 870-879.
- 12. Kirschner, K., et al., Functional heterogeneity in senescence. Biochem Soc Trans, 2020. 48(3): p. 765-773.
- Liu, Y., et al., Senescence in osteoarthritis: from mechanism to potential treatment. Arthritis Research & Earpy, 2022. 24(1).
- Astrike-Davis, E.M., P. Coryell, and R.F. Loeser, Targeting cellular senescence as a novel treatment for osteoarthritis. Current Opinion in Pharmacology, 2022. 64.
- Houtman, E., et al., Elucidating mechano-pathology of osteoarthritis: transcriptome-wide differences in mechanically stressed aged human cartilage explants. Arthritis Res Ther, 2021. 23(1): p. 215.
- Houtman, E., et al., Human Osteochondral Explants: Reliable Biomimetic Models to Investigate Disease Mechanisms and Develop Personalized Treatments for Osteoarthritis. Rheumatol Ther, 2021. 8(1): p. 499-515.
- 17. Chen, Z., et al., Cellular senescence in ionizing radiation (Review). Oncology Reports, 2019.
- 18. Li, M., et al., Ionizing Radiation-Induced Cellular Senescence in Normal, Non-transformed Cells and the Involved DNA Damage Response: A Mini Review. Front Pharmacol, 2018. 9: p. 522.
- Wang, Y., M. Boerma, and D. Zhou, Ionizing Radiation-Induced Endothelial Cell Senescence and Cardiovascular Diseases. Radiat Res, 2016. 186(2): p. 153-61.
- Cash, H. and D. Dean, The effects of low-dose radiation on articular cartilage: a review. Journal of Biological Engineering, 2019. 13(1).
- 21. Bomer, N., et al., Neo-cartilage engineered from primary chondrocytes is epigenetically similar to autologous cartilage, in contrast to using mesenchymal stem cells. Osteoarthritis and Cartilage, 2016. 24(8): p. 1423-1430.
- 22. Debacq-Chainiaux, F., et al., Protocols to detect senescence-associated beta-galactosidase (SA-betagal) activity, a biomarker of senescent cells in culture and in vivo. Nat Protoc, 2009. 4(12): p. 1798-806.
- Mankin, H.J., et al., Biochemical and metabolic abnormalities in articular cartilage from osteo-arthritic human hips. II. Correlation of morphology with biochemical and metabolic data. J Bone Joint Surg Am, 1971. 53(3): p. 523-37.
- 24. Boone, I., et al., Identified senescence endotypes in aged cartilage are reflected in the blood metabolome.

- GeroScience, 2023.
- Ramos, Y.F.M., et al., Genes Involved in the Osteoarthritis Process Identified through Genome Wide Expression
  Analysis in Articular Cartilage; the RAAK Study. PLoS ONE, 2014. 9(7): p. e103056.
- Coutinho De Almeida, R., et al., RNA sequencing data integration reveals an miRNA interactome of osteoarthritis
  cartilage. Annals of the Rheumatic Diseases, 2019. 78(2): p. 270-277.
- Tuerlings, M., et al., RNA Sequencing Reveals Interacting Key Determinants of Osteoarthritis Acting in Subchondral Bone and Articular Cartilage: Identification of IL11 and CHADL as Attractive Treatment Targets. Arthritis & Rheumatology, 2021. 73(5): p. 789-799.
- 28. Chen, Z., et al., Cellular senescence in ionizing radiation (Review). Oncol Rep, 2019. 42(3): p. 883-894.
- 29. Pignolo, R.J., S.F. Law, and A. Chandra, Bone Aging, Cellular Senescence, and Osteoporosis. JBMR Plus, 2021. 5(4).
- Saul, D., et al., A new gene set identifies senescent cells and predicts senescence-associated pathways across tissues. Nature Communications, 2022. 13(1).
- D'Costa, S., M.J. Rich, and B.O. Diekman, Engineered Cartilage from Human Chondrocytes with Homozygous Knockout of Cell Cycle Inhibitor p21. Tissue Engineering Part A, 2020. 26(7-8): p. 441-449.
- Georget, M., et al., Development of a DNA damage-induced senescence model in osteoarthritic chondrocytes. Aging, 2023. 15(17): p. 8576-8593.
- Copp, M.E., et al., The combination of mitogenic stimulation and DNA damage induces chondrocyte senescence.
   Osteoarthritis and Cartilage, 2021. 29(3): p. 402-412.
- Rodríguez Ruiz, A., et al., Cartilage from human-induced pluripotent stem cells: comparison with neo-cartilage from chondrocytes and bone marrow mesenchymal stromal cells. Cell and Tissue Research, 2021. 386(2): p. 309-320.

# **Supplementary Material**

### Supplementary Methods Osteochondral Explants and human in-vitro cartilage organoid model

Osteochondral explants and cells were taken from joints obtained from OA patients in the Research Arthritis and Articular Cartilage (RAAK) study. In this study, joint material, for example cartilage and bone tissue, was collected from patients who underwent a total joint replacement surgery due to OA. Explants (diameter of 8 mm) were taken from the weight bearing condyles of knee joints for the osteochondral explant culture as described previously <sup>18,19</sup>. In short, biopsies with a diameter of 8 mm, were taken from the macroscopically normal cartilage from OA patients and washed in PBS. The thickness of the cartilage and bone varied between donors. Next, the explants were cultured in serum-free chondrogenic differentiation medium containing DMEM (Gibco), with ascorbid acid (Sigma-Aldrich), L-proline (Sigma-Aldrich), sodium pyruvate (Sigma-Aldrich), dexamethasone (Sigma-Aldrich), ITS+ (Corning) and pen/strepp (Gibco).

The human primary articular chondrocytes (hPACs) were collected and cultured as described previously  $^{24}$ . In short, macroscopically normal cartilage was treated overnight in medium with 2 mg/ml collagenase type 1 (Worthington) in a humidified 5% CO $_2/37^{\circ}$ C incubator. After which the cells were taken and filtered to remove cell and tissue debris and cultured in serum-free chondrogenic differentiation medium. Subsequently, the human *in-vitro* cartilage organoids were formed using 500 g centrifugal forces on a 96 wellsplate with 5 x10 $^{\circ}$  cells per well. 100  $\mu$ l serum-free chondrogenic differentiation medium with 10 ng/ml TGF- $\beta$ 1 (peprotech) was used for the culture of the cartilage organoids. In this experiment a total of 142 explants from 29 donors were included

and cells from 3 additional donors were used for the human *in-vitro* cartilage organoids. Donor characteristics are described in Supplementary Table S1.

### Irradiation and loading regime

As seen in Supplementary Figure S1, three days after extraction, explants were placed in sterile PBS and irradiated with 20 Gy (Yxlon, Germany). After 5 days, dynamic unconfined compression was applied using the MACH-1 (Biomomentum Inc., Laval, QC, Canada) apparatus for 4 days. During this dynamic loading, a strain of 65% with a frequency of 1 Hz was applied to the explants for 10 minutes. At day 12, the explants were harvested. First a cross-section of cartilage/bone was taken from the center of the explant for IHC, after which the cartilage was separated from the bone and snap-frozen in liquid nitrogen. The samples were stored at -80 dC for further analysis. The human in-vitro cartilage organoids were exposed to 10 or 20 Gy ionizing radiation on day 7 of the culture and on day 10 the cartilage organoids were harvested for IHC. Four cartilage organoids were pooled and stored in TRIzol reagent (Invitrogen, San Diego, CA) at -80 dC for gene expression analysis. In total 143 osteochondral explants were used from 29 donors, divided in control (n=31 osteochondral explants, N=29 donors), irradiation (n = 16 osteochondral explants and N = 12 donors), hyper physiological mechanical loading (n = 20 osteochondral explants and N = 18 donors) and combination group(n = 42 osteochondral explants and N = 29 donors).

### Gene expression

Osteochondral explants and human *in-vitro* cartilage organoids were processed and RNA was extracted as described previously <sup>18,19</sup>. In summary, the osteochondral explants were pulverized using a Mixer mill 200 (Retch, Germany) in TRIzol reagent. RNA was extracted from the osteochondral explants and *in-vitro* cartilage organoids using the RNeasy Mini Kit (Qiagen, GmbH, Hilden, Germany). The quantity of RNA was assessed and cDNA synthesis was performed. Gene expression was measured using RT-qPCR, with the Biomark<sup>TM</sup> 96.96 Dynamic Arrays (Fluidigm) according to the manufacturer's protocol and with the QuantStudio 6 Real-Time PCR system (Applied Biosystems). *POU6F1* and *HECTD3* were used as housekeeping genes. All genes measured using RT-qPCR and their primer sequence are listed in Supplementary table S2.

### Statistical analysis

Statistical tests were performed using SPSS (v.29). Significance was determined using unpaired Generalized Estimating equations (GEE) with multivariate analysis. Genes were taken as dependent variable, models were taken as independent variable and there was corrected for RT-qPCR analysis type and donor. Controls were taken as baseline.

### Histology

For the senescence associated beta galactosidase (SA-β-gal) staining, the explants were washed with PBS and fixed for 15 minutes at 4 dC using 4% formaldehyde with 0.5% glutaraldehyde. The explants were washed and incubated for 24 hours at 37dC with the staining solution as described previously <sup>25</sup>. The staining solution contained 0.5M Potassium hexacyanoferrate(III) (Merck), 0.5M Potassium hexacyanoferrate(II) trihydrate (Merck), 1M Magnesium chloride hexahydrate (Merck), 5M Sodium Chloride (Merck), 0.1M Citric acid monohydrate (Merck), 0.2M Dibasic sodium phosphate dihydrate (Merck) were mixed and pH was set to 6. Subsequently, 2% X-gal (Sigma) was added fresh to the staining solution before incubation. After incubation, the explants were washed

and decalcified for 10 days at 37°C with Mol-Decalcifier (Milestone). Subsequently, the explants were embedded in TissueTek (Sakura) and sectioned. Slides were washed and counterstained with nuclear fast red (Sigma) for 5 minutes. Next, the slides were dehydrated, cleared and fixated using Pertex (Sigma). Slides were imaged with the Zeiss Axioscan Z1 slide scanner, using a 10x magnification. Images were processed using ImageJ (v.1.53c). When chondrocytes were blue they were considered SA- $\beta$ -gal positive. 4 random areas were selected per cartilage section (Supplementary Figure S2E). 2 sections were measured per condition and the total number of SA- $\beta$ -gal positive cells were counted and averaged.

For the cartilage quality score (Mankin score), explants were fixed for 24 hours at 4°C, subsequently decalcified and sectioned as described above. Tissue sections were stained with Haematoxylin & Eosin Y (H&E) or Toluidine Blue (Sigma-Aldrich), as described previously <sup>18</sup> and scored for cartilage integrity by using the Mankin score and two independent reviewers <sup>26</sup>.

To indicate apoptotic cells in the tissue, the Click-iT™ Plus TUNEL assay kit was used (Invitrogen). Explants were fixed for 24 hours at 4°C, subsequently decalcified and sectioned as described above. In short, first a TdT reaction was performed, where modified dUTP is incorporated at the 3' end of the fragmented DNA. Subsequently, the Click-iT™ plus reaction was performed, where the fluorescent dye is added to the dUTP group, and DAPI was used as counter stain. Slides were imaged with the Zeiss Axioscan Z1 slide scanner, using a 10x magnification. Images were processed using ImageJ (v.1.53c). Per tissue, 4 random areas were selected and averaged per condition (N= 2 donors). The TUNEL-positive cells were counted as apoptotic cells and the DAPI- positive cells were used as the total number of cells.

#### References

- Houtman, E., et al., Elucidating mechano-pathology of osteoarthritis: transcriptome-wide differences in mechanically stressed aged human cartilage explants. Arthritis Res Ther, 2021. 23(1): p. 215.
- Houtman, E., et al., Human Osteochondral Explants: Reliable Biomimetic Models to Investigate Disease Mechanisms and Develop Personalized Treatments for Osteoarthritis. Rheumatol Ther, 2021. 8(1): p. 499-515.
- Bomer, N., et al., Neo-cartilage engineered from primary chondrocytes is epigenetically similar to autologous cartilage, in contrast to using mesenchymal stem cells. Osteoarthritis and Cartilage, 2016. 24(8): p. 1423-1430.
- Debacq-Chainiaux, F., et al., Protocols to detect senescence-associated beta-galactosidase (SA-betagal) activity, a biomarker of senescent cells in culture and in vivo. Nat Protoc, 2009. 4(12): p. 1798-806.
- Mankin, H.J., et al., Biochemical and metabolic abnormalities in articular cartilage from osteo-arthritic human hips. II. Correlation of morphology with biochemical and metabolic data. J Bone Joint Surg Am, 1971. 53(3): p. 523-37.

# Supplementary data

**Table S1** - Patients characteristics of osteochondral explants and high-throughput neo-cartilage mini pellets. %F = percentage Females; Age is in years; KL score = Kellgren-Lawrence score, a OA severity score.

	Osteochondral explants	Mini-pellets
	(Gene expression, N=29)	(Gene expression, N=3)
Female/Male	22/7	2/1
%F	75.9	66.7
Age (s.d.)	70.1 (7.5)	65.0 (3.0)
KL score (s.d.)	3.9 (0.3)	4.0 (0)
Knees (Hips)	30 (0)	3 (0)

Table S2 - Genes measured with qPCR.

Gene	Name	Function	Primer sequences forward/reverse
POU6F1	POU Class 6 Homeobox 1	Housekeeping gene	5'-CAGTTGGTGTCCAAGCCACAT-3' /5'-CTTGGCAAACTCCCGGATCT-3'
HECTD3	HECT Domain E3 Ubiquitin Protein Ligase 3	Housekeeping gene	5'-CCGACATGGACCTACGAGTG-3' / 5'-CACGTTGAACTCCTCCGTGT-3'
COL2A1	Collagen type 2	Cartilage qualtity	5'-CTACCCCAATCCAGCAAACGT-3' / 5'-AGGTGATGTTCTGGGAGCCTT-3'
ACAN	Aggrecan	Cartilage quality	5'-AGAGACTCACACAGTCGAAACAGC-3' / 5'-CTATGTTACAGTGCTCGCCAGTG-3'
COL1A1	Collagen type 1	Bone quality/ anabolic marker	5' - GTGCTAAAGGTGCCAATGGT-3' / 5'-ACCAGGTTCACCGCTGTTAC -3'
DMP1	Dentin Matrix Acidic Phosphoprotein 1	Osteocyte marker	5'-TGAACTACGGAGGGTAGAGGT-3' / 5'-ACCTGGTTACTGGGAGAGCA-3'
MEPE	Matrix Extracellular Phosphoglycoprotein	Osteocyte marker	5'-GGCCAGTGACTGCGATTAAAC-3' / 5'-CCTTCGAGTGTGCTTTAGCAT-3'
CTSK	Cathepsin K	Osteoclast marker	5'-TTCCCGCAGTAATGACACCC-3' / 5'-GGAACCACACTGACCCTGAT-3'
RUNX2	RUNX Family Transcription Factor 2	Osteoblast marker	5'-CTGTGGTTACTGTCATGGCG-3' / 5'-AGGTAGCTACTTGGGGAGGA-3'
ALPL	Alkaline Phosphatase	Osteoblast marker	5'-CAAAGGCTTCTTCTTGCTGGTG-3' / 5'-CCTGCTTGGCTTTTCCTTCA-3'
CDKN1A	Cyclin Dependent Kinase Inhibitor 1A	Cell cycle inhibitor/ senescence marker/ DNA damage/ p21 pathway	5'-CTGGAGACTCTCAGGGTCGA-3' / 5'-CTTCCTGTGGGCGGATTAGG-3'
CDKN2A	Cyclin Dependent Kinase Inhibitor 2A	Cell cycle inhibitor/ senescence marker/ p16 pathway	5'-TGCCCAACGCACCGAATAG-3' / 5'-GCCCATCATCATGACCTGGAT-3'

Gene	Name	Function	Primer sequences forward/reverse
GADD45A	Growth Arrest And DNA Damage Inducible Alpha	Senescence marker/ DNA damage	5'-GCGAGAACGACATCAACATCC-3' / 5'-AATGTGGATTCGTCACCAGCA-3'
MKI67	Marker Of Proliferation Ki-67	Senescence marker/ Cell proliferation marker	5'-ACACATTGTCCTCAGCCTTCT-3' / 5'-GTGCCTGAGATCAAGAAAGACA-3'
LMNB1	Lamin B1	Cell cycle inhibitor/ senescence marker/ DNA damage	5'-GGAGCAGACTTACCATGCCA-3' / 5'-TGCGGCTTTCCATCAGTTCT-3'
HMGB1	High Mobility Group Box 1	Cell cycle inhibitor/ senescence marker	5'-TGCCTCGCTGAGGAAAAATA-3' / 5'-TTTGCCTCTCGGCTTCTTAGG-3'
IL6	Interleukin 6	SASP marker	5'-GGTACATCCTCGACGGCATC-3' / 5'-TGTTTTCTGCCAGTGCCTCT-3'
IL8	Interleukin 8	SASP marker	5'-GGCAGCCTTCCTGATTTCTG-3' / 5'-CTTGGCAAAACTGCACCTTCAC-3'
SERPINE1	Serpin Family E Member 1	SASP marker	5'-TGAGGGTGTTTCAGCAGGTG-3' / 5'-GTGAGAAAACCACGTTGCGG-3'
IGFBP3	Insulin Like Growth Factor Binding Protein 3	SASP marker	5'-AAAAGCAGTGTCGCCCTTCC-3' / 5'-TCCTTCCCCTTGGTGGTGTA-3'
IGFBP6	Insulin Like Growth Factor Binding Protein 6	SASP marker	5'-GTCTACCGAGGGGCTCAAAC-3' / 5'-GACTTGCCCATCCGATCCAC-3'
MMP3	Matrix Metallopeptidase 3	SASP marker	5'-CTGGACTCCGACACTCTGGA-3' / 5'-CAGGAAAGGTTCTGAAGTGACC-3'
MMP13	Matrix Metallopeptidase 13	SASP marker/ OA marker	5'-TTGAGCTGGACTCATTGTCG-3' / 5'-GGAGCCTCTCAGTCATGGAG-3'

Table S3 - Quantification of TUNEL staining. 4 squares per donor were averaged, 2 donors were used per condition. N=2

Condition	Cartilage	Bone
Control	20%(17%)	60%(61%)
IR	19%(13%)	55%(32%)
ML	16%(11%)	109%(62%)
IRML	23%(17%)	87%(40%)

4 squares per donor were averaged, 2 donors were used per condition. N=2

Table S4 - Effect ionizing radiation in the high-throughput neo-cartilage

Irradiation						
	FC (SD)	Beta	P-value			
Cartilage anabolism			,			
COL2A1	0.7 (0.2)	-0.5	2.5x10 <sup>-02</sup>			
ACAN	0.5 (0.2)	-1.0	1.6x10 <sup>-05</sup>			
Positive senescence markers						
CDKN1A	4.6 (2.0)	2.3	1.6x10 <sup>-33</sup>			
CDKN2A	0.8 (0.5)	-0.3	3.9x10 <sup>-01</sup>			

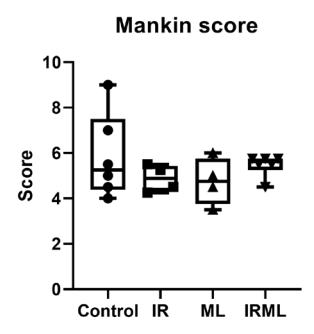
Irradiation							
	FC (SD)	Beta	P-value				
GADD45A	1.9 (0.0)	1.2	4.6x10 <sup>-18</sup>				
Negative senescence markers							
LMNB1	0.1 (0.1)	-2.9	3.7x10 <sup>-11</sup>				
SASP markers							
IL6	0.1 (0.0)	0.2	7.2x10 <sup>-01</sup>				
IL8	0.6 (1.2)	-1.0	1.5x10 <sup>-01</sup>				
SERPINE1	0.9 (0.2)	-0.2	7.1x10 <sup>-02</sup>				
IGFBP3	1.0 (0.3)	0.1	8.0x10 <sup>-01</sup>				
IGFBP6	1.1 (0.4)	0.2	1.2x10 <sup>-01</sup>				
MMP3	0.6 (0.3)	-0.5	3.3x10 <sup>-01</sup>				
MMP13	0.5 (0.8)	-0.9	1.8x10 <sup>-01</sup>				

Notes: GEE test, FC= $2^{-ddCT}$ , SD= standard deviation, Beta= estimate of the GEE test. P-value<0.05 is considered significant, n = 5-31 neo-cartilage organoid pellets, N = 1-3 donors.

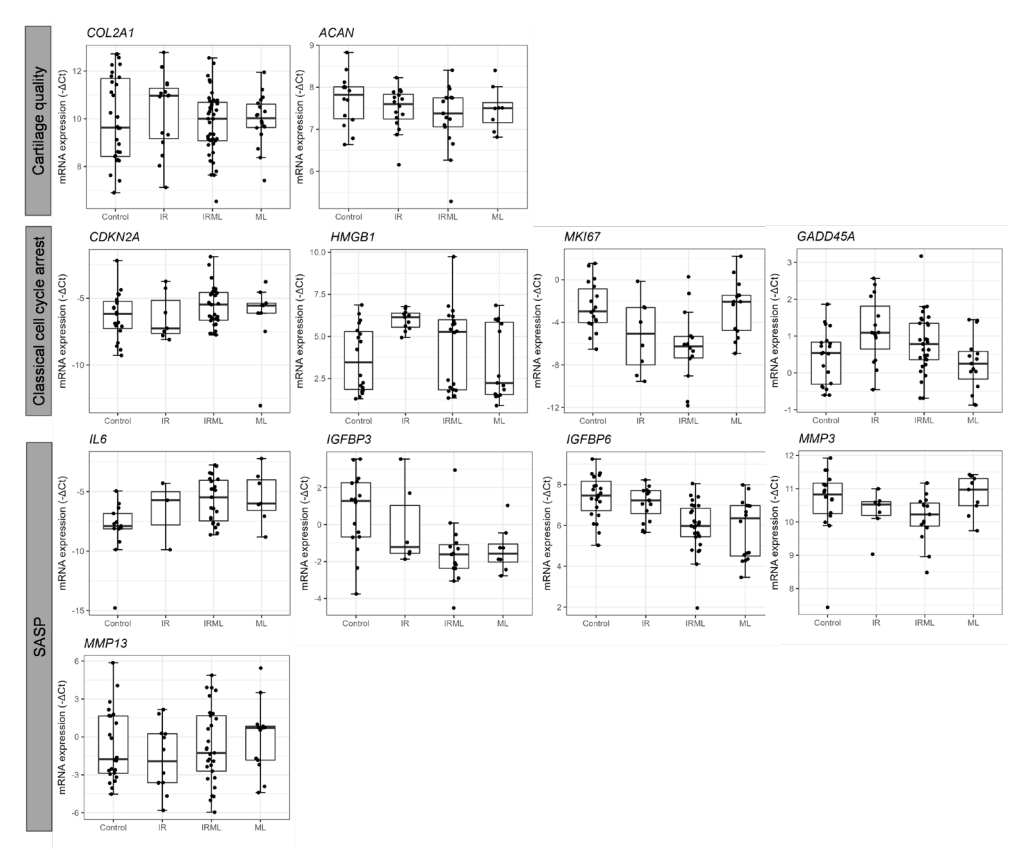
Table S5 - Gene expression fold changes between preserved and lesioned cartilage reflecting OA pathophysiology.

	Cartilag	e			Bone				
Gene name	OA pathophysiology*		Seneso stress	Senescence Mechanical stress		OA pathophysiology*		Senescence Mechanical stress	
	FC	FDR	FC	P-value	FC	FDR	FC	P-value	
CDKN2A	1,1	8,2x10 <sup>-01</sup>	1,3	9,1x10 <sup>-02</sup>	0,8	2,0x10 <sup>-01</sup>	1,1	5,9x10 <sup>-01</sup>	
CDKN1A	1,1	6,5x10 <sup>-01</sup>	0,8	3,6x10 <sup>-01</sup>	0,9	6,0x10 <sup>-01</sup>	1,2	1,6x10 <sup>-01</sup>	
GADD45A	0,9	3,9x10 <sup>-01</sup>	0,9	5,6x10 <sup>-01</sup>	0,9	5,5x10 <sup>-01</sup>	0,9	2,2x10 <sup>-04</sup>	
MKI67	2,1	2,9x10 <sup>-03</sup>	0,8	9,3x10 <sup>-01</sup>	1,3	2,4x10 <sup>-01</sup>	0,8	2,3 x10 <sup>-01</sup>	
LMNB1	1,5	7,6x10 <sup>-02</sup>	1	8,8x10 <sup>-01</sup>	1,2	1,1x10 <sup>-01</sup>	1,1	2,5x10 <sup>-01</sup>	
HMGB1	1,2	4,3x10 <sup>-01</sup>	1,1	4,3x10 <sup>-01</sup>	1,0	7,2x10 <sup>-01</sup>	1,1	7,0x10 <sup>-01</sup>	
IL6	0,6	4,1x10 <sup>-01</sup>	3,6	5,8x10 <sup>-02</sup>	1,0	7,5x10 <sup>-01</sup>	1,2	4,7x10 <sup>-02</sup>	
IL8	1,0	9,5x10 <sup>-01</sup>	2	2,2x10 <sup>-02</sup>	0,8	4,7x10 <sup>-01</sup>	1,3	1,9x10 <sup>-01</sup>	
SERPINE1	3,0	2,2x10 <sup>-10</sup>	1,9	7,8x10 <sup>-03</sup>	1,4	1,2x10 <sup>-01</sup>	1,4	2,8x10 <sup>-01</sup>	
IGFBP3	2,7	1,1x10 <sup>-07</sup>	0,3	1,5x10 <sup>-03</sup>	0,8	2,6x10 <sup>-02</sup>	0,8	1,3x10 <sup>-04</sup>	
IGFBP6	1,4	7,8x10 <sup>-02</sup>	0,4	3,9x10 <sup>-05</sup>	1,0	9,0x10 <sup>-01</sup>	0,8	3,8x10 <sup>-03</sup>	
MMP3	0,5	2,8x10 <sup>-07</sup>	0,8	1,0x10 <sup>-01</sup>	0,9	8,6x10 <sup>-01</sup>	1,5	7,4x10 <sup>-01</sup>	
MMP13	0,9	8,3x10 <sup>-01</sup>	1,5	8,9x10 <sup>-01</sup>	1,2	6,4x10 <sup>-01</sup>	6,3	5,4x10 <sup>-14</sup>	

\*OA pathophysiology as determined by the difference in gene expression between preserved (reference) and lesioned OA affected tissue (N=30 pairs) 1-3 Senescence Mechanical stress as determined by the difference in gene expression between the control explants and the SASP model in cartilage, n = 16-51 osteochondral explants, N = 12-29 donors. FC = foldchange, FDR= P-value corrected for multiple testing, P-value<0.05 is considered significant.



 $\textbf{Figure S1} - \textbf{Cartilage quality score (Mankin score) of the different models. n = 30 osteochondral explants, N=6 donors. \\ \textbf{IR= irradiation model, ML = Hyper physiological mechanical loading model, IRML= combination model.}$ 



 $\begin{tabular}{l} {\bf Figure~S2} - {\bf Cartilage~gene~expression~of~the~different~models.~n=16-51~osteochondral~explants, N=12-29~donors.~IR=irradiation~model, ML=Hyper~physiological~mechanical~loading~model, IRML=~combination~model. \end{tabular}$ 

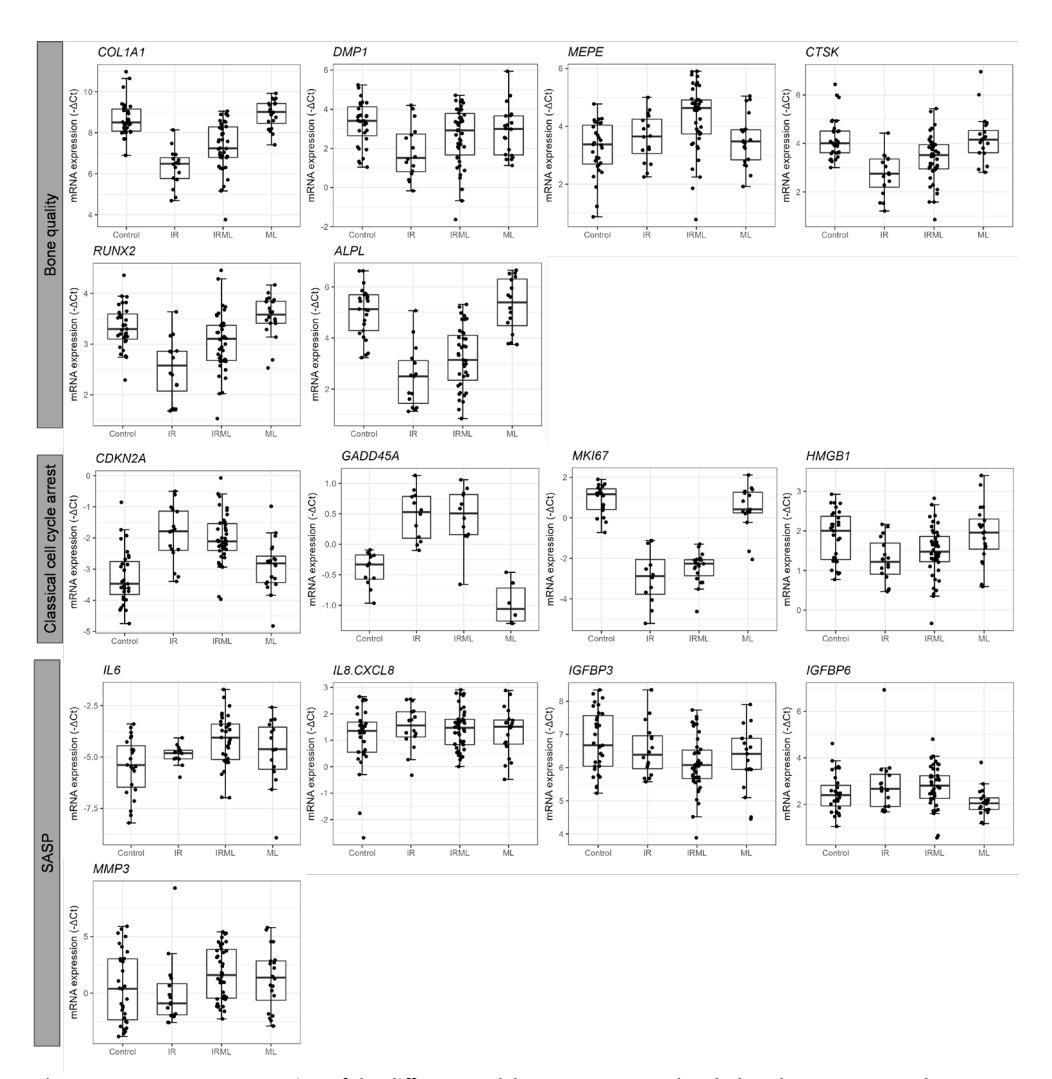


**Figure S3** - Bone gene expression of the different models. n = 16-51 osteochondral explants, N = 12-29 donors. IR= irradiation model, ML = Hyper physiological mechanical loading model, IRML= combination model.

## References

- Coutinho De Almeida, R., et al., RNA sequencing data integration reveals an miRNA interactome of osteoarthritis cartilage. Annals of the Rheumatic Diseases, 2019. 78(2): p. 270-277.
- 2. Ramos, Y.F.M., et al., Genes Involved in the Osteoarthritis Process Identified through Genome Wide Expression Analysis in Articular Cartilage; the RAAK Study. PLoS ONE, 2014. 9(7): p. e103056.
- Tuerlings, M., et al., RNA Sequencing Reveals Interacting Key Determinants of Osteoarthritis Acting in Subchondral Bone and Articular Cartilage: Identification of IL11 and CHADL as Attractive Treatment Targets. Arthritis & Rheumatology, 2021. 73(5): p. 789-799.